ACS APPLIED MATERIALS & INTERFACES

Research Article

www.acsami.org

One-Step Thermal-Treatment Route to Fabricate Well-Dispersed ZnO Nanocrystals on Nitrogen-Doped Graphene for Enhanced Electrochemiluminescence and Ultrasensitive Detection of Pentachlorophenol

Ding Jiang,[†] Xiaojiao Du,[‡] Qian Liu,[‡] Lei Zhou,[‡] Jing Qian,[‡] and Kun Wang*[,‡]

[†]School of Food and Biological Engineering, Jiangsu University, Zhenjiang, 212013, P. R. China

[‡]Key Laboratory of Modern Agriculture Equipment and Technology, School of Chemistry and Chemical Engineering, Jiangsu University, Zhenjiang, 212013, P. R. China

Supporting Information

ABSTRACT: Heteroatom doping enables graphene with novel properties and thus may broaden the potential of graphene-based materials. In this paper, novel ZnO-nanocrystal-decorated nitrogen-doped graphene (N-GR) composites were prepared through a one-step thermal-treatment route using glycine as the nitrogen source. ZnO nanocrystals with a size about 8 nm were well-dispersed and tightly anchored on the N-GR sheet. Compared with ZnO-nanocrystal-decorated undoped graphene, the ZnO/N-GR nanocomposites could not only enhance the electrochemiluminescence (ECL) intensity by 4.3-fold but also moved the ECL onset potential positively for ~200 mV. All these results could be ascribed to the presence of nitrogen in graphene which decreased the barrier of ZnO nanocrystals reduction. Furthermore, the ECL sensor based on ZnO/N-GR nanocomposites was fabricated for the ultrasensitive detection of pentachlorophenol (PCP). This recyclable and eco-friendly sensor has excellent performances including wide linear range (0.5 pM to ~61.1 nM), low detection limit (0.16 pM, S/N = 3), good selectivity, and stability, which is a promising sensor for practical application in environment analysis.

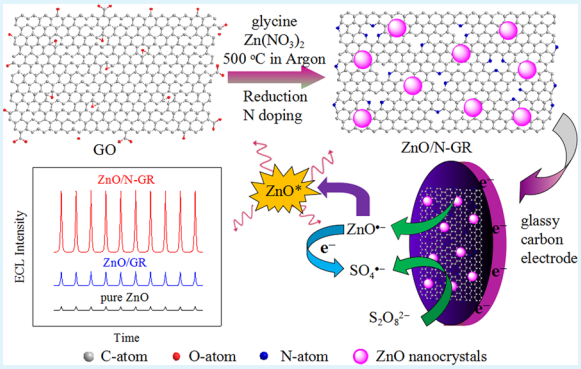

KEYWORDS: *ZnO nanocrystal, nitrogen-doped graphene, electrochemiluminescence, pentachlorophenol, detection*

1. INTRODUCTION

Zinc oxide (ZnO) has gained increasing research attention in recent years, with many potential proof-of-concept device demonstrations such as field effect transistors,[1] transparent conductors,[2] ultraviolet light-emitting diodes,[3] and especially chemical sensors.[4−9] For chemical sensors, previous studies of traditional metal oxides indicated that the sensing performance has been correlated with structures.[10,11] ZnO may have the richest variety of different structures, which is a benefit for sensor design and fabrication. To date, ZnO nanostructures (such as nanorods, nanotubes, nanocrystals, and combs) have been employed in immunosensor, enzyme biosensor, and other type sensors.[4−7] Especially, ZnO nanocrystals (also called quantum dots[7]) have shown excellent sensing performances owing to their unique advantages such as high catalytic efficiency, good chemical stability, strong adsorption ability, and unique optical and electronic properties.[8,9] For instance, Bai et al. synthesized ZnO nanocrystals through a mild sol−gel method and then fabricated a gas sensor. This sensor showed the highest response to NO_2 and exhibited high selectivity over CO and CH_4.[8] Ng's group prepared ZnO nanocrystals by a facile sol−gel hydrolysis method and then fabricated a miniature fluorescent probe to detect Cu^{2+} in aqueous medium, which exhibited low detection limit, high sensitivity, and fast response time.[9]

Previous studies have proved that ZnO nanocrystals typically have two disadvantages which restrict their practical applications:[12] (1) ZnO nanocrystals are not stable and easy to aggregate because of their large specific surface area and high surface activity and (2) they are not available for practical applications because the suspended nanocrystals are easily lost during the reaction. To overcome these disadvantages of ZnO nanocrystals, researchers have made great efforts to introduce ZnO nanocrystals on/into supports (such as silica nanotubes, carbon nanotubes, graphene, and so on) to form nanocomposites.[12−15] Among these materials, two-dimensional (2D) carbon atom−graphene has attracted significant attention due to its high theoretical specific surface area, good thermal

Received: October 16, 2014
Accepted: January 21, 2015
Published: January 21, 2015

DOI: 10.1021/am507163z
ACS Appl. Mater. Interfaces 2015, 7, 3093−3100

conductivity, excellent electrical conductivity, and unique optical properties.[16−18] More importantly, incorporation of ZnO nanocrystals onto graphene sheets can provide greater versatility in carrying out selective sensing processes or enhanced sensing performances.[14,15] For example, Zeng's group developed room temperature formaldehyde sensors based on ZnO-nanocrystal-decorated graphene nanocomposites which exhibited enhanced performance, excellent selectivity, and good stability.[14] Guo et al. fabricated a graphene-based device on the basis of ZnO-nanocrystal-decorated graphene and found that the electrical response was largely enhanced by 2−3 orders.[15]

Recently, nitrogen-doped graphene (N-GR), as a novel kind of graphene derived 2D material, has received considerable interest by virtue of its excellent properties owing to the introduction of nitrogen atoms. Compared with pristine graphene and other carbonaceous materials, the special 2D structures of N-GR with heteroatomic defects and disordered surface morphology shows improved electrical conductivity, thermal stability, and specific surface area.[19,20] Further, N-GR composite structures synergistically integrated with other components, such as polymers and biomolecules, metal−metal oxide nanoparticles, may offer novel properties which could be potentially useful for some different purposes.[21] Thus, the combination of ZnO nanocrystals and the special 2D carbon-based material N-GR at the nanoscale dimension may attract a flurry of activities. However, as far as we know, there is no report that graphene can be decorated with ZnO nanocrystals and nitrogen doped in one step via thermal treatment route.

Electrochemiluminescence (ECL) is the optical emission from the excited states of an ECL luminophore produced at an electrode surface via electrochemical high-energy electron transfer reaction.[22] As an important detection method, ECL has been widely applied in analytical chemistry owing to its low background signal, versatility, high stability, and sensitivity.[23,24] All-solid-state ECL sensors have been widely studied, because they can not only reduce the consumption of reagents but also simplify the experimental process. So far, most of the ECL sensors were fabricated on the basis of inorganic semiconductor nanocrystals (such as CdS and CdSe) as reagents for ECL generation.[25−29] However, the ECL sensors based on Zn-based II−VI semiconductors have rarely been investigated because of the instability and the wide band gap. In recent years, Geng et al. have investigated the ECL behaviors of Zn-based II−VI semiconductor nanostructures in aqueous systems.[29] Although they have achieved a reasonably good stability, the ECL intensities of these nanomaterials are relatively low. Thus, more detailed investigations of the ECL behaviors for Zn-based nanomaterials are urgently needed.

In this work, ZnO-nanocrystal-decorated N-GRs were prepared via one-step thermal-treatment route by using glycine (Gly) as the nitrogen source. Meanwhile, Gly could promote the reduction of oxy-functional groups on the surface of graphene oxide, resulting in fewer anchoring sites in N-GR for formation of well-dispersed ZnO nanocrystals. Compared with ZnO-nanocrystal-decorated undoped graphene (ZnO/GR), the ZnO/N-GR could not only enhance the ECL intensity by 4.3-fold but also moved the onset ECL potential more positively for about 200 mV. Moreover, a novel ECL sensor has been constructed, which showed excellent performances for pentachlorophenol (PCP) sensing with high sensitivity, good selectivity, wide detection range, and good stability. The proposed ECL sensor extended the application of N-GR and ZnO nanocrystals and could be a promising method for the routine monitoring of PCP in environment.

2. EXPERIMENTAL SECTION

2.1. Reagents and Chemicals. Graphite was purchased from Qingdao Tianhe Graphite Co., Ltd. Nafion (5 wt % solution in lower aliphatic alcohol), PCP, 3-monochlorophenol (3-CP), 1,3,5-trichlorobenzene (1,3,5-TCP), and 2,4-dichlorophenol (2,4-DCP) were purchased from Sigma-Aldrich. Phosphate buffer solutions (PBS, 0.1 M) were prepared from NaOH, Na_2HPO_4, and NaH_2PO_4. PBS with various pH were made up by titrating 0.1 M H_3PO_4 or 0.1 M NaOH. GO was prepared using modified Hummers method from graphite powders.[30] Doubly distilled water was used throughout this work. All other reagents were of analytical reagent grade.

2.2. Apparatus. Transmission electron microscope (TEM) images were performed by using a JEOL JSM-6700 transmission electron microscope (Tokyo, Japan). Scanning electron microscopy (SEM) images and energy-dispersive spectra (EDS) were performed on a Hitachi S4800 scanning electron equipped with an energy-dispersive spectrum (EDS) spectrometer (INCA x-act, UK). Atomic absorption spectra (AAS) were attained by using an atomic absorptionspectrophotometer (Purkinje General TAS-986, China). X-ray diffraction (XRD) spectra was conducted using Cu target with a Panalytical high resolution XRD-1, PW 3040/60 unit. Raman spectra were performed on a Renishaw InVia Raman spectrometer with an excitation wavelength at 785 nm. X-ray photoelectron spectroscopy (XPS) was conducted on a Thermo VG Scientific ESCALAB 250 spectrometer using a Mg Kα radiator. Electrochemical impedance spectra (EIS) were conducted using ZENNIUM electrochemical workstation in 0.1 M KCl solution containing 5 mM $Fe(CN)_6^{3-/4-}$ with the frequency range from 0.01 Hz to 10 kHz. The ECL measurements were obtained using a model MPI-A electro-chemiluminescence analyzer (Xi'an Remex Analysis Instrument Co. Ltd. Xi'an, China) with 800 V photomultiplier tube voltage. The conventional three-electrode system was employed with a modified glassy carbon electrode (GCE, 3 mm) as the working electrode, a Pt wire as the counter electrode, and a Ag/AgCl (saturated with KCl) as the reference electrode.

2.3. Preparation of ZnO/N-GR Nanocomposites, ZnO/GR Nanocomposites, and ZnO. ZnO/N-GR nanocomposites were synthesized by one-step thermal-treatment (as shown in Scheme 1).

Scheme 1. Schematic Illustration for the Preparation of ZnO/N-GR

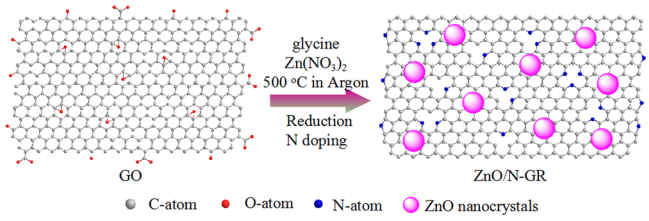

Typically, 5 mg of GO was dispersed in 5 mL of twice-distilled water through sonication for several minutes to give a brown solution. After 10 mg of Gly and 10 mg of $Zn(NO_3)_2$ were added into the as-prepared solution, the mixture was sonicated for several hours and then poured into an alumina crucible. Under argon atmosphere, the temperature of the mixture was gradually increased to 500 °C and then maintained for 2 h. Finally, the products could be directly collected from the alumina crucible. For comparison, the ZnO/GR nanocomposites and pure ZnO were synthesized with the same process except for the addition of Gly or GO, respectively.

2.4. Preparation of ZnO/N-GR Nanocomposites, ZnO/GR Nanocomposites, and ZnO Modified Electrodes. Primarily, the GCE was first polished with sand paper followed by 1.0, 0.3, and 0.05 μm alumina slurry, respectively. After sonication in ethanol and double distilled water, respectively, the electrode was rinsed with twice-

DOI: 10.1021/am507163z
ACS Appl. Mater. Interfaces 2015, 7, 3093−3100

distilled water and allowed to dry at room temperature. A 2 mg mL^{-1} ZnO/N-GR suspension was prepared by dispersing 2.0 mg of ZnO/N-GR in 1.0 mL of ethanol with ultrasonic agitation for about 10 min. Then 6 μL of the as-prepared suspension was dropped on the electrode surface and dryed in ambient air for 24 h. In order to entrap the sample, 6 μL of Nafion solution (0.5 wt % in ethanol) was covered on it and also dryed in ambient air for 24 h. Nafion-ZnO/N-GR modified GCE was thus successfully obtained (denoted as Nafion-ZnO/N-GR/GCE). For comparison, in order to keep the constant amount of ZnO, 1.67 mg mL^{-1} ZnO/GR suspension and 1.06 mg mL^{-1} ZnO suspension were prepared, respectively. Then Nafion-ZnO/GR/GCE and Nafion-ZnO/GCE were prepared using a similar procedure.

3. RESULTS AND DISCUSSION

3.1. Characterization of the Samples. XRD patterns of ZnO, ZnO/GR, and ZnO/N-GR are shown in Figure 1. For sample ZnO, several diffraction peaks appeared ranging from 30−70°, which could be indexed as the wurtzite phase of ZnO (PDF No. 36-1451).[8,14] In the case of ZnO/GR and ZnO/N-GR, a typical pattern of wurtzite phase for ZnO could also be identified, and a new broad peak at ~26.5° appeared, indicating the presence of graphene sheets in the nanocomposites.[31,32] All these peaks were relatively wide, which implied the small size of ZnO nanocrystals. Moreover, there was no significant differences observed in the XRS spectra between ZnO/GR and ZnO/N-GR, suggesting nitrogen doping has little effect on the crystal phase of ZnO.

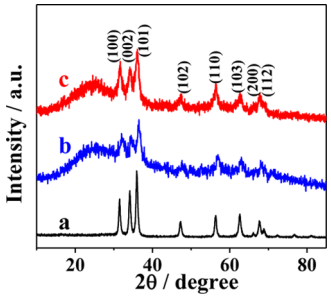

Figure 1. XRD patterns of pure ZnO (a), ZnO/GR (b), and ZnO/N-GR (c).

To characterize the structure and morphology of the as-prepared nanocomposites, SEM and TEM observations were conducted. The SEM images revealed that the ZnO nanocrystals were homogeneously attached on the N-GR surfaces (Figure 2A,B). Additionally, the EDS spectra of ZnO/N-GR were obtained in Figure 2C, which confirmed the presence of C, N, O, and Zn. Figure 2D displayed a TEM image of the ZnO/N-GR at a lower magnification, which further confirmed that the as-prepared ZnO/N-GR were made of ZnO nanocrystals and transparent N-GR thin films. The high-magnification TEM image of ZnO/N-GR (Figure 2E) revealed that the ZnO nanocrystals ranging from 4−10 nm were well dispersed on the thin N-GR layers. The relatively good distribution and high-coverage of ZnO nanocrystals on the N-GR could guarantee excellent electrochemical performances and good stability of ZnO/N-GR. Figure 2F showed the lattice-resolved HRTEM image of ZnO nanocrystals, which exhibited lattice spacing of 0.25 and 0.28 nm, corresponding to the (101) and (100) crystal planes of ZnO, respectively.[13,33] For comparison, the morphology of ZnO/GR was also characterized by TEM. As shown in Figures S1A and S1B, the outlines of GR and ZnO NPs were hard to be clearly observed, and ZnO nanocrystals tended to agglomerate, indicating that nitrogen doping was helpful for the uniform dispersion of ZnO nanocrystals on the graphene surface. As we know, there are a large number of oxygen-containing functional groups on the surface of GO, which could be used as anchoring sites during the formation of metal oxides.[32] During the ZnO/N-GR preparation, Gly could promote the reduction of oxy-functional groups on the surface of graphene oxide.[34] N-GR has fewer sites than graphene for anchoring ZnO nanocrystals. So comparing to those nanocrystals decorated on graphene, ZnO nanocrystals loaded on N-GR had a better dispersion. Moreover, the EDS spectra of ZnO/GR was also obtained in Figure S1C, and it was clear that the nitrogen could not be found in ZnO/GR, which indicated that the nitrogen in graphene was derived from Gly. In addition, the Zn^{2+} contents were 52.86% and 63.47% for ZnO/N-GR and ZnO/GR as determined by ASS, respectively, which

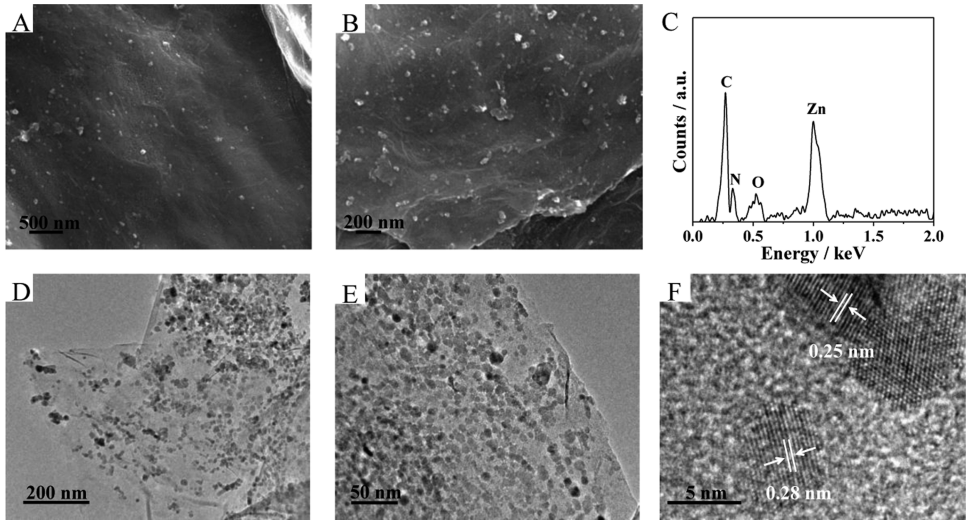

Figure 2. (A) Low-magnification SEM image of ZnO/N-GR. (B) High-magnification SEM image of ZnO/N-GR. (C) EDS spectrum of ZnO/N-GR. (D) Low-magnification TEM image of ZnO/N-GR. (E) High-magnification TEM image of ZnO/N-GR. (F) High-resolution image of ZnO nanocrystals in ZnO/N-GR.

DOI: 10.1021/am507163z
ACS Appl. Mater. Interfaces 2015, 7, 3093−3100

supports that N-GR has fewer sites than graphene for anchoring ZnO nanocrystals.

Raman spectra were applied to the characterization of the quality and structure of carbon-based nanomaterials, especially to investigate the defects, the disordered and ordered structures of graphene. The typical Raman spectra of the ZnO/N-GR nanocomposites were displayed in Figure 3. For a comparison,

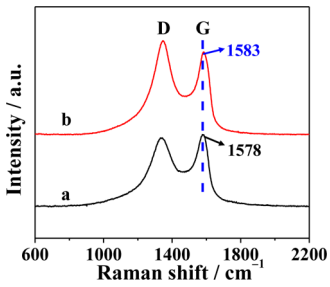

Figure 3. Raman spectra of graphene (a) and ZnO/N-GR (b).

the graphene spectrum obtained from thermal reduction of GO in the same conditions was also shown. It is obvious that two remarkable peaks of graphene were observed at 1343 and 1577 cm^{-1}, which was attributed to the D and G bands of graphene-based materials, respectively. The D band is associated with structural defects, while the G band can be attributed to the result of the first-order scattering of the E_{2g} mode of sp^2 carbon domains.[31,32] Compared with graphene, the ZnO/N-GR exhibited a strong D band peak at 1343 cm^{-1} because of the existence of defects caused by N-doping in the graphene sheet. Moreover, the G band of the ZnO/N-GR shifted to 1583 cm^{-1}, indicating the effect of nitrogen doping.[35] It is widely recognized that the ratio of relative intensity for D and G band (I_D/I_G) could be used as the measure for the extents of defects in graphene-based materials. The ZnO/N-GR revealed higher intensity ratio of I_D/I_G (1.13) than graphene (0.88), which indicated that there were large amounts of defects in the nanocomposites.[36] The defects of graphene might be favorable to improve the electrochemical properties of the nanocomposites.

To understand the composition and chemical nature of ZnO/N-GR nanocomposite, XPS measurements have been performed. As shown in Figure 4A, the XPS spectrum suggested that the sample contained C, N, O, and Zn elements, which provided evidence for nitrogen doping into the graphene sheets. The high-resolution scan of Zn 2p in Figure 4B showed that the two peaks that appeared at 1022.7 and 1045.7 eV could be attributed to Zn $2p_{3/2}$ and Zn $2p_{1/2}$ peaks, respectively, which confirmed the existence of ZnO in the nanocomposites.[8,12] The deconvoluted C 1s XPS spectrum (Figure 4C) showed four peaks at 284.8, 285.9, 287.2, and 289.1 eV, representing sp^2-sp^2C, N-sp^2C, N-sp^3C, and C−O type bonds, respectively.[37,38] In the spectrum of N 1s (Figure 4D), the broad peak could be fitted into two peaks at 398.6 and 399.8 eV, which were ascribed to the pyridine nitrogen and pyrrolic nitrogen atoms in the nanocomposites.[36] The pyridinic nitrogen in ZnO/N-GR could provide a couple of electrons to the π-conjugated rings, introducing the properties of electron donor into graphene-based materials; the pyrrolic nitrogen has faster charge mobility in N-GR owing to its better electron-donor properties.[32,38] Notably, the amount of nitrogen incorporated in ZnO/N-GR was found to be approximately 4.8% with a relatively high doping level, which could greatly

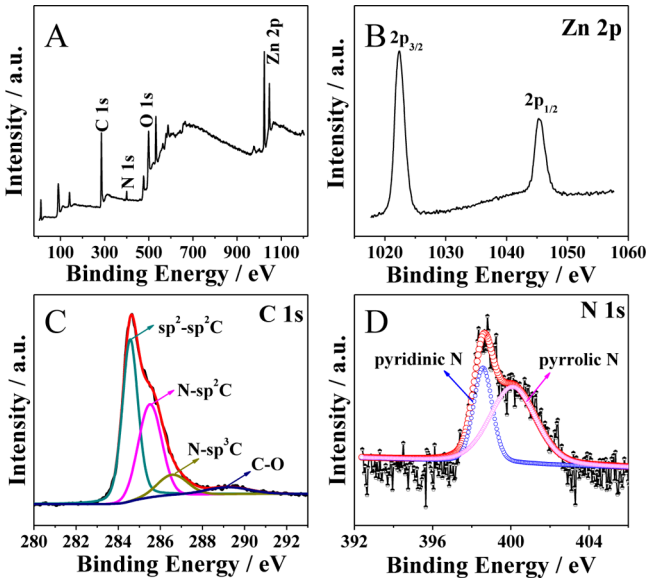

Figure 4. (A) XPS survey spectra of ZnO/N-GR. (B) Zn 3d XPS spectrum of the ZnO/N-GR. (C) The high-resolution XPS spectra of the C 1s region for ZnO/N-GR. (D) The high-resolution XPS spectra of the N 1s region for ZnO/N-GR.

increase the electrochemical activity and electrical conductivity of the nanocomposites. Thus, the ZnO/N-GR nanocomposites are expected to improve the electrochemical performances. The XPS spectrum of ZnO/GR prepared in the same conditions without Gly was shown in Figure S2. It was obviously that the sample of ZnO/GR has no N 1s peak, indicating that the N atoms were derived from Gly and could be doped in graphene lattices by thermal treatment. Therefore, we could conclude that the deposition of ZnO on graphene and the nitrogen doping of graphene were realized in a facile step by our method.

Based on the discussion above, it could be concluded that ZnO/N-GR nanocomposites were fabricated through a one-step thermal-treatment route. While ZnO nanocrystals were anchored on the N-GR surface, nitrogen doping was achieved simultaneously. In the preparation process of ZnO/N-GR, the Gly played important roles in serving as the nitrogen source and simultaneously prompting the reduction of oxygen-containing functional groups on the surface of GO. As a source for nitrogen doping, it could be confirmed that there was no obvious nitrogen content in the controlled experiment without Gly. Furthermore, as Mayavan et al. reported, Gly was utilized as the fuel to reduce NO_3^-, inducing the decomposition for the mixture of Gly-nitrate. The decomposition products could prompt the reduction of GO,[34] with the result that N-GR can load well-dispersed ZnO nanocrystals.

3.2. Electrochemical and ECL Behaviors of As-Synthesized Nanocomposites. Electrochemical impedance spectrum (EIS) is a vital tool for investigating the interface properties of the modified electrodes, which normally includes a semicircular portion and a linear portion. It is usually considered that the semicircle diameter is the equivalent of the electron-transfer resistance (R_{et}), which acts as an important role in the electron transfer kinetics of the redox probe.[39] Figure 5 exhibits the impedance spectra of different modified electrodes in 0.1 M KCl with 5 mM $Fe(CN)_6^{3-/4-}$ ions, respectively. The bare GCE showed an almost straight line (curve a), implying the characteristic of a diffuse limiting step of

DOI: 10.1021/am507163z
ACS Appl. Mater. Interfaces 2015, 7, 3093−3100

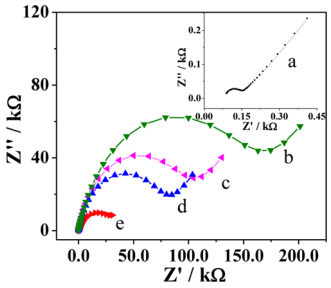

Figure 5. Electrochemical impedance spectra of bare GCE (a), Nafion/GCE (b), Nafion-ZnO/GCE (c), Nafion-ZnO/GR/GCE (d), and Nafion-ZnO/N-GR/GCE (e) in 0.1 M KCl containing 5 mM $Fe(CN)_6^{3-/4-}$.

the electrochemical processes. After dripping Nafion on the electrode surface, an obvious interfacial R_{et} was observed (curve b) since Nafion could act as a barrier to block the interfacial charge transfer. The R_{et} of the Nafion-ZnO/GR/GCE (curve d) is much smaller than those of Nafion-GCE (curve b) and Nafion-ZnO/GCE (curve c), revealing the graphene could serve as an excellent electron-transfer interface between the electrode and the electrochemical probe. Moreover, when the ZnO/N-GR nanocomposites were incorporated into the electrochemical system, we discovered that the diameter decreased further (curve e), indicating the N-GR could accelerate the electron-transfer more effective, which is attributed to the nitrogen in graphene.[32,38]

,

Cyclic voltammograms (CVs) of the Nafion/GCE, Nafion-ZnO/GCE, Nafion-ZnO/GR/GCE and Nafion-ZnO/N-GR/GCE were recorded in 0.1 M pH 7.0 PBS between 0.0 and −2.0 V, as shown in Figure S3. For Nafion/GCE, there were no apparent reduction currents, implying that the CVs collected in the experiments followed were not affected by the electrolysis of water. While Nafion-ZnO/GCE, Nafion-ZnO/GR/GCE, and Nafion-ZnO/N-GR/GCE (curves b, c, and d) showed a reduction potential of ZnO.[40] Moreover, compared with pure ZnO, the cathodic peak current of ZnO/N-GR increased and the reduction potential shifted positively, which indicated that the N-GR in ZnO/N-GR nanocomposites decreased the potential barrier of ZnO.[40]

ECL emission measurements were carried out with CVs in 0.1 M pH 7.0 PBS containing 0.1 M $K_2S_2O_8$ at different electrodes between 0 and −2.0 V, as displayed in Figure 6. According to a previous study, nanocrystals could be oxidized and reduced by charge injection at the surface of the electrodes

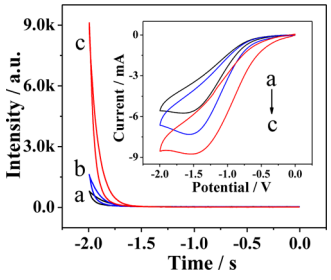

Figure 6. ECL-potential curves of Nafion-ZnO/GCE (a), Nafion-ZnO/GR/GCE (b), and Nafion-ZnO/N-GR/GCE (c) in 0.1 M PBS (pH 7.0) containing 50 mM $K_2S_2O_8$ (scan rate 200 mV s^{-1}). Inset: the corresponding CVs of them.

during the potential cycling.[41] Herein the ECL was on the base of the electron-transfer process between oxidized species of the coreactant ($SO_4^{\bullet-}$) and reduced species formed in ZnO. While the negative potential was applied to the modified electrode, $S_2O_8^{2-}$ was reduced and generated a strong oxidant $SO_4^{\bullet-}$, and then $SO_4^{\bullet-}$ reacted with the electro-generated species ($ZnO^{\bullet-}$) to produce higher intensity ECL emission.[40,42] The whole process could be stated as follows:

$$ZnO + ne^- \rightarrow nZnO^{\cdot-}$$

$$S_2O_8^{2-} + e^- \rightarrow SO_4^{2-} + SO_4^{\cdot-}$$

$$ZnO^{\cdot-} + SO_4^{\cdot-} \rightarrow ZnO^* + SO_4^{2-}$$

$$ZnO^* \rightarrow ZnO + h\nu$$

The data of onset potentials and ECL intensity for ZnO/N-GR nanocomposites, ZnO/GR nanocomposites, and pure ZnO were summarized in Table 1. It could be seen that the onset

Table 1. Summary of ECL Measurements of ZnO/N-GR, ZnO/GR, and Pure ZnO

	ZnO/N-GR	ZnO/GR	pure ZnO
ECL onset potential/V	−1.35	−1.53	−1.62
ECL intensity/a.u.	9150	2145	627

potentials of ECL for the ZnO/N-GR nanocomposites and the ZnO/GR nanocomposites are more positive than that of pure ZnO. Moreover, compared with the ZnO/GR nanocomposites, the ZnO/N-GR nanocomposites could move the ECL onset potential more positively for ~200 mV. Because the ECL onset potential could be ascribed to the potential barrier of ZnO reduction, this suggests that ZnO particles on N-GR were more readily reduced than particles on graphene. Furthermore, the ECL intensity from the ZnO/N-GR nanocomposites was about 4.3-fold higher than that of the ZnO/GR nanocomposites. From the inset of Figure 6, CVs demonstrated that the cathodic peak current was greatly enhanced and the onset reduction potential of ZnO also shifted positively in the ZnO/N-GR nanocomposites than those of ZnO/GR nanocomposites, which demonstrated that the N-GR in ZnO/N-GR nanocomposites could reduce the potential barriers of ZnO. Meanwhile, N-GR with high conductivity would produce more $SO_4^{\bullet-}$ and then improved the quantity of ZnO*, which could also increase the ECL intensity.

In addition, we have investigated the effect of different nitrogen contents on ECL performance. Composites with different nitrogen contents were prepared by simply adjusting the addition of Gly during the synthesis process. As shown in Figure S4, the nitrogen contents were 0.9%, 2.7%, and 4.8% for ZnO/N-GR-1, ZnO/N-GR-2, and ZnO/N-GR-3 as determined by XPS, respectively. However, the nitrogen content cannot increase greater than 4.8% by further increasing the amount of Gly in this work. ECL emission measurements were carried out, and the related data were summarized in Table S1. It could be seen that the ECL intensity increased significantly with the increase of nitrogen contents. Therefore, ZnO/N-GR with 4.8% N content was used in the following experiments.

3.3. Fabrication of the ECL Sensing Platform for PCP.

Based on the robust ECL signal, the fabricated Nafion-ZnO/N-GR/GCE was applied in the PCP detection. PCP has been extensively used in industry and agriculture as a component of herbicides, bactericides, insecticides, preservatives, and bio-

DOI: 10.1021/am507163z
ACS Appl. Mater. Interfaces 2015, 7, 3093−3100

cides.[43] It is actually poisonous, and the accumulation of PCP in living organisms will induce deleterious effects such as carcinogenicity and acute toxicity.[43,44] Thus, it is of great importance to develop sensors to detect PCP. Accordingly, we tried to fabricate a novel ECL sensor to detect PCP based on ZnO/N-GR nanocomposites.

Prior to the detection of PCP, some experimental conditions which affected the ECL intensity were optimized. Apparently, as a coreactant ECL system, the ECL intensity of Nafion-ZnO/N-GR/GCE was related with the concentration of the $S_2O_8^{2-}$. As shown in Figure S5A, the ECL intensity increased significantly with the concentration of $S_2O_8^{2-}$ increase in the range from 0 to 0.05 M. The reason might be attributed to the fact that more ZnO* was produced from the oxidation of $ZnO^{\bullet-}$ by the electrogenerated $SO_4^{\bullet-}$. However, further increase in $K_2S_2O_8$ concentration caused the decrease of ECL intensity because the excess $S_2O_8^{2-}$ would easily react with the negatively charged ZnO which inhibited the formation of the ZnO*. The phenomenon was similar to a previous study.[45] Accordingly, 0.05 M was chosen as the optimal concentration of $K_2S_2O_8$ in this work. The ECL intensity of Nafion-ZnO/N-GR/GCE could also be influenced by the scan rates. As shown in Figure S5B, The ECL intensity increased steadily with the scan rates increased from 25 to 200 mV/s and then decreased while the scan rates were higher than 200 mV/s. As stated in previous reports, high scan rates could promote the consumption of $K_2S_2O_8$, leading to the decrease of ECL signal.[45,46] Therefore, 100 mV/s was chosen in the following experiments.

The pH value was another important factor for the sensing system which could affected obviously the ECL intensity. As shown in Figure S5C, the ECL signal increased when the pH increased from 5.0 to 7.0 and dropped at higher pH. As we know, at the negative potential, it was easy to reduce the proton at lower pH and then the electro-reduction of ZnO was inhibited. While at pH 9.0, the strong oxidant $SO4^{\bullet-}$ was consumed by OH^- owing to the scavenging effect.[45,47] Therefore, pH 7.0 was selected in the following experiments.

Excellent stability is one of the main points for extending potential application in the sensing field. Figure 7 displayed the

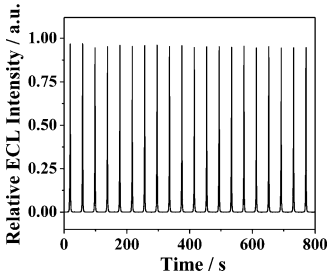

Figure 7. Stability of ECL emissions from the Nafion-ZnO/N-GR/GCE under 20 continuous cycles of CV scan.

ECL intensities of the Nafion-ZnO/N-GR/GCE under 20 repeated CV scans under the optimal conditions. The ECL intensity from ZnO/N-GR was pretty stable with the relative standard deviation of 0.36%, which indicated that the sensing signal was quite reliable.

Figure 8A showed that the ECL intensity decreased obviously with the PCP concentration increasing. As shown in Figure 8B, the relative ECL intensity change of $\Delta I/I_0$ was linear related to the logarithm of the PCP concentration

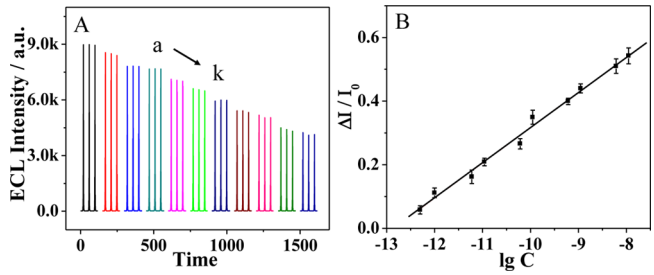

Figure 8. (A) ECL response of Nafion-ZnO/N-GR/GCE upon addition of serial concentrations of PCP in 0.1 M PBS under the optimal conditions. (B) The linear calibration curve for PCP determination.

ranging from 0.5 pM to 61.1 nM with the correlation coeffcient of 0.995 and the limit of detection (LOD) of 0.16 pM (S/N = 3) (where I_0 was the initial ECL intensity without PCP and ΔI was the decreased ECL intensity that PCP-induced). The achieved LOD in our work was much lower than those published reports, which were summarized in Table S2. Moreover, this sensor showed much superiority in PCP detecting, such as simple, fast operation, low-cost, and environmental friendliness, which indicated that the as-prepared ECL sensor had great potential applications in the environmental monitoring and analysis.

The detection of PCP has been reported on the basis of the quenching effect on the ECL of carbon quantum dots.[48,49] Similarly, the ECL quenching mechanism of PCP here might be attributed to electron transfer annihilation of $ZnO^{\bullet-}$. Scheme 2

Scheme 2. Schematic Showing the ECL Detection of PCP with Nafion-ZnO/N-GR/GCE

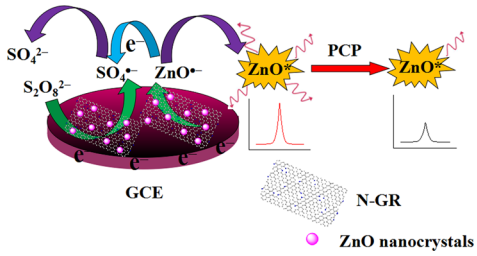

intuitively showed the mechanism. At first, electrons were transferred from the surface of the electrode to ZnO and $S_2O_8^{2-}$ through N-GR, resulting the formation of $ZnO^{\bullet-}$ and $SO_4^{\bullet-}$. The ECL signal was generated from the generation of ZnO* through the electron transfer annihilation of $ZnO^{\bullet-}$ and $SO_4^{\bullet-}$. When PCP was added, it would be adsorbed on the surface of N-GR and then consumed $ZnO^{\bullet-}$, leading to the decrease of ECL signal.

Furthermore, the specifity of this ECL sensor was studied using PCP, 3-CP, 1,3,5-TCP, 2,4-DCP, and several common ions as the interferents. As shown in Figure S6, only PCP quenched the ECL emission of Nafion-ZnO/N-GR/GCE dramatically, whereas the analogs of PCP quenched the ECL emission slightly (e.g., 3-CP, 1,3,5-TCP, and 2,4-DCP). The reason might be attributed that the analogs of PCP were oxidized with difficulty by excited-state ZnO due to their more stable chemical properties, which was similar to previous study.[48,49] Moreover, the inorganic interferences hardly had effects on the ECL intensity (e.g., Na^+, K^+, Mg^{2+}, Ca^{2+}, Fe^{3+},

DOI: 10.1021/am507163z
ACS Appl. Mater. Interfaces 2015, 7, 3093−3100

Cl^-, NO_3^-, and SO_4^{2-}). All these results showed that the sensing platform had high selectivity toward PCP.

4. CONCLUSIONS

In summary, we have successfully prepared ZnO/N-GR nanocomposites by a facile method through thermal treatment. SEM and TEM characterizations showed that ZnO nanocrystals ranging from 4−10 nm were homogeneously attached on the surface of N-GR. Compared with ZnO/GR, the ECL intensity of ZnO/N-GR could be 4.3-fold, and the onset potential of ECL moved positively for ∼200 mV due to the introduction of nitrogen in graphene. Then a new ECL sensing method was established based on ZnO/N-GR, which displayed excellent performances for PCP detection, such as high stability, low detection limit, wide linear range, and good specificity to PCP. This work proposed a significant method to design MO_x/N-GR nanocomposites and expand their applications in electrochemical sensors.

■ ASSOCIATED CONTENT

Supporting Information

TEM images, EDS spectrum, and XPS survey spectra of ZnO/GR. Effects of nitrogen contents, $K_2S_2O_8$ concentration, pH, and scan rates on the ECL intensity of the Nafion-ZnO/N-GR/GCE. Comparison of methods for the determination of PCP. Selectivity of the Nafion-ZnO/N-GR/GCE based sensor for PCP detection over other interferences under the optimal conditions. This material is available free of charge via the Internet at http://pubs.acs.org.

■ AUTHOR INFORMATION

Corresponding Author

*Tel.: +86 511 88791800. Fax: +86 511 88791708. E-mail: wangkun@ujs.edu.cn.

Notes

The authors declare no competing financial interest.

■ ACKNOWLEDGMENTS

This work was supported by the National Natural Science Foundation of China (Nos. 21175061, 21375050, and 21405062), China Postdoctoral Science Foundation (no. 2014M551507), Key Laboratory of Modern Agriculture Equipment and Technology (No. NZ201109), a Project Funded by the Priority Academic Program Development of Jiangsu Higher Education Institutions (No. PAPD-2014-37), and Qing Lan Project.

■ REFERENCES

(1) Wang, X. D.; Zhou, J.; Song, J. H.; Liu, J.; Xu, N. S.; Wang, Z. L. Piezoelectric Field Effect Transistor and Nanoforce Sensor Based on a Single ZnO Nanowire. *Nano Lett.* **2006**, *12*, 2768−2772.

(2) Jaramillo, R.; Ramanathan, S. Electronic Granularity and the Work Function of Transparent Conducting ZnO:Al Thin Films. *Adv. Funct. Mater.* **2011**, *21*, 4068−4072.

(3) Chien, J. F.; Liao, H. Y.; Yu, S. F.; Lin, R. M.; Shiojiri, M.; Shyue, J. J.; Chen, M. J. Ultraviolet Electroluminescence from Nitrogen-Doped ZnO-Based Heterojuntion Light-Emitting Diodes Prepared by Remote Plasma in situ Atomic Layer-Doping Technique. *ACS Appl. Mater. Interfaces* **2013**, *5*, 227−232.

(4) Dorfman, A.; Kumar, N.; Hahm, J. I. Nanoscale ZnO-Enhanced Fluorescence Detection of Protein Interactions. *Adv. Mater.* **2006**, *18*, 2685−2690.

(5) Asif, M. H.; Nur, O.; Willander, M.; Danielsson, B. Selective Calcium Ion Detection with Functionalized ZnO Nanorods-Extended Gate MOSFET. *Biosens. Bioelectron.* **2009**, *24*, 3379−3382.

(6) Dai, Z. H.; Shao, G. J.; Hong, J. M.; Bao, J. C.; Shen, J. Immobilization and Direct Electrochemistry of Glucose Oxidase on a Tetragonal Pyramid-Shaped Porous ZnO Nanostructure for a Glucose Biosensor. *Biosens. Bioelectron.* **2009**, *24*, 1286−1291.

(7) Sergiu, V. N.; Daniela, G.; Mariana, S.; Leona, C. N. Sequential Thermal Decomposition of the Shell of Cubic ZnS/$Zn(OH)_2$ Core-Shell Quantum Dots Observed With Mn^{2+} Probing Ions. *J. Phys. Chem. C* **2013**, *117*, 22017−22028.

(8) Bai, S. L.; Hu, J. W.; Li, D. Q.; Luo, R. X.; Chen, A. F.; Liu, C. C. Quantum-Sized ZnO Nanoparticles: Synthesis, Characterization and Sensing Properties for NO_2. *J. Mater. Chem.* **2011**, *21*, 12288−12294.

(9) Ng, S. M.; Wong, D. S. N.; Phung, J. H. C.; Chua, H. S. Integrated Miniature Fluorescent Probe to Leverage the Sensing Potential of ZnO Quantum Dots for the Detection of Copper (II) Ions. *Talanta* **2013**, *116*, 514−519.

(10) Qian, J.; Yang, X. W.; Jiang, L.; Zhu, C. D.; Mao, H. P.; Wang, K. Facile Preparation of Fe_3O_4 Nanospheres/Reduced Graphene Oxide Nanocomposites with High Peroxidase-Like Activity for Sensitive and Selective Colorimetric Detection of Acetylcholine. *Sens. Actuators, B* **2014**, *201*, 160−166.

(11) Rahman, M. M.; Ahammad, A. J. S.; Jin, J. H.; Ahn, S. J.; Lee, J. J. A Comprehensive Review of Glucose Biosensors Based on Nanostructured Metal-Oxides. *Sensors* **2010**, *10*, 4855−4886.

(12) Zhang, X.; Shao, C. L.; Zhang, Z. Y.; Li, J. H.; Zhang, P.; Zhang, M. Y.; Mu, J. B.; Guo, Z. C.; Ling, P. P.; Liu, Y. C. In situ Generation of Well-Dispersed ZnO Quantum Dots on Electrospun Silica Nanotubes with High Photocatalytic Activity. *ACS Appl. Mater. Interfaces* **2012**, *4*, 785−790.

(13) Dutta, M.; Basak, D. Photosensitization of Multiwalled Carbon Nanotube Scaffolds with ZnO Quantum Dots for Photovoltaic Applications. *J. Nanopart. Res.* **2011**, *13*, 5311−5319.

(14) Huang, Q. W.; Zeng, D. W.; Li, H. Y.; Xie, C. S. Room Temperature Formaldehyde Sensors with Enhanced Performance, Fast Response and Recovery Based on Zinc Oxide Quantum Dots/Graphene Nanocomposites. *Nanoscale* **2012**, *4*, 5651−5658.

(15) Guo, W. H.; Xu, S. G.; Wu, Z. F.; Wang, N.; Loy, M. M. T.; Du, S. W. Oxygen-Assisted Charge Transfer Between ZnO Quantum Dots and Graphene. *Small* **2013**, *18*, 3031−3036.

(16) Kamat, P. V. J. Phys. Chem. Lett. Graphene and Graphene Oxide: Synthesis, Properties, and Applications. *Adv. Mater.* **2010**, *1*, 520−527.

(17) Mei, Q. S.; Zhang, Z. P. Photoluminescent Graphene Oxide Ink to Print Sensors onto Microporous Membranes for Versatile Visualization Bioassays. *Angew. Chem., Int. Ed.* **2012**, *51*, 5602−5606.

(18) Yang, L.; Zhang, R. L.; Liu, B. H.; Wang, J. P.; Wang, S. H.; Han, M. Y.; Zhang, Z. P. π-Conjugated Carbon Radicals at Graphene Oxide to Initiate Ultrastrong Chemiluminescence. *Angew. Chem., Int. Ed.* **2014**, *53*, 10109−10113.

(19) Wang, H. B.; Maiyalagan, T.; Wang, X. Review on Recent Progress in Nitrogen-Doped Graphene: Synthesis, Characterization, and Its Potential Applications. *ACS Catal.* **2012**, *2*, 781−794.

(20) Wang, H. B.; Xie, M. S.; Thia, L.; Fisher, A.; Wang, X. Strategies on the Design of Nitrogen-Doped Graphene. *J. Phys. Chem. Lett.* **2014**, *5*, 119−125.

(21) Lee, W. J.; Maiti, U. N.; Lee, J. M.; Lim, J.; Han, T. H.; Kim, S. O. Nitrogen-Doped Carbon Nanotubes and Graphene Composite Structures for Energy and Catalytic Applications. *Chem. Commun.* **2014**, *50*, 6818−6830.

(22) Richter, M. Electrochemiluminescence (ECL). *Chem. Rev.* **2004**, *104*, 3003−3036.

(23) Wang, X. F.; Zhou, Y.; Xu, J. J.; Chen, H. Y. Signal-On Electrochemiluminescence Biosensors Based on CdS-Carbon Nanotube Nanocomposite for the Sensitive Detection of Choline and Acetylcholine. *Adv. Funct. Mater.* **2009**, *19*, 1444−1450.

(24) Li, Q.; Zheng, J. Y.; Yan, Y. L.; Zhao, Y. S.; Yao, J. N. Electrogenerated Chemiluminescence of Metal-Organic Complex

DOI: 10.1021/am507163z
ACS Appl. Mater. Interfaces 2015, 7, 3093−3100

Nanowires: Reduced Graphene Oxide Enhancement and Biosensing Application. *Adv. Mater.* **2012**, *24*, 4745−4749.
(25) Liu, B.; Ren, T.; Zhang, J. R.; Chen, H. Y.; Zhu, J. J.; Burda, C. Spectroelectrochemistry of Hollow Spherical CdSe Quantum Dot Assemblies in Water. *Electrochem. Commun.* **2007**, *9*, 551−557.
(26) Wang, C. Z.; Fan, L. Z.; Wang, Z. H.; Liu, H. B.; Li, Y. L.; Yang, S. H.; Li, Y. L. Directed Assembly of Hierarchical CdS Nanotube Arrays from CdS Nanoparticles: Enhanced Solid State Electrochemiluminescence in H_2O_2 Solution. *Adv. Mater.* **2007**, *19*, 3677−3681.
(27) Wang, K.; Liu, Q.; Wu, X. Y.; Guan, Q. M.; Li, H. N. Graphene Enhanced Electrochemiluminescence of CdS Nanocrystal for H_2O_2 Sensing. *Talanta* **2010**, *82*, 372−376.
(28) Zou, G. Z.; Ju, H. X. Electrogenerated Chemiluminescence from a CdSe Nanocrystal Film and Its Sensing Application in Aqueous Solution. *Anal. Chem.* **2004**, *76*, 6871−6878.
(29) Geng, J.; Liu, B.; Xu, L.; Hu, F. N.; Zhu, J. J. Facile Route to Zn-Based II-VI Semiconductor Spheres, Hollow Spheres, and Core/Shell Nanocrystals and Their Optical Properties. *Langmuir* **2007**, *23*, 10286−10293.
(30) Gilje, S.; Han, S.; Wang, M. S.; Wang, K. L.; Kaner, R. B. A Chemical Route to Graphene for Device Applications. *Nano Lett.* **2007**, *11*, 3394−3398.
(31) Zhang, Z. Y.; Xiao, F.; Guo, Y. L.; Wang, S.; Liu, Y. Q. One-Pot Self-Assembled Three-Dimensional TiO_2-Graphene Hydrogel with Improved Adsorption Capacities and Photocatalytic and Electrochemical Activities. *ACS Appl. Mater. Interfaces* **2013**, *5*, 2227−2233.
(32) Yang, S. H.; Song, X. F.; Zhang, P.; Gao, L. Facile Synthesis of Nitrogen-Doped Graphene-Ultrathin MnO_2 Sheet Composites and Their Electrochemical Performances. *ACS Appl. Mater. Interfaces* **2013**, *5*, 3317−3322.
(33) Park, S.; An, S.; Ko, H.; Jin, C.; Lee, C. M. Synthesis of Nanograined ZnO Nanowires and Their Enhanced Gas Sensing Properties. *ACS Appl. Mater. Interfaces* **2012**, *4*, 3650−3656.
(34) Mayavan, S.; Sim, J. B.; Choi, S. M. Easy Synthesis of Nitrogen-Doped Graphene-Silver Nanoparticle Hybrids by Thermal Treatment of Graphite Oxide with Glycine and Silver Nitrate. *Carbon* **2012**, *50*, 5148−5155.
(35) Guo, B.; Liu, Q.; Chen, E.; Zhu, H.; Fang, L.; Gong, J. R. Controllable N-Doping of Graphene. *Nano Lett.* **2010**, *10*, 4975−4980.
(36) Zhang, K. J.; Han, P. X.; Gu, L.; Zhang, L. X.; Liu, Z. X.; Kong, Q. X.; Zhang, C. J.; Dong, S. M.; Zhang, Z. Y.; Yao, J. H.; Xu, H. X.; Cui, G. L.; Chen, L. Q. Synthesis of Nitrogen-Doped MnO/Graphene Nanosheets Hybrid Material for Lithium Ion Batteries. *ACS Appl. Mater. Interfaces* **2012**, *4*, 658−664.
(37) Zhang, C. H.; Fu, L.; Liu, N.; Liu, M. H.; Wang, Y. Y.; Liu, Z. F. Synthesis of Nitrogen-Doped Graphene Using Embedded Carbon and Nitrogen Sources. *Adv. Mater.* **2011**, *23*, 1020−1024.
(38) Jiang, D.; Liu, Q.; Wang, K.; Qian, J.; Dong, X. Y.; Yang, Z. T.; Du, X. J.; Qiu, B. J. Enhanced Non-Enzymatic Glucose Sensing Based on Copper Nanoparticles Decorated Nitrogen-Doped Graphene. *Biosens. Bioelectron.* **2014**, *54*, 273−278.
(39) Kang, X. H.; Wang, J.; Wu, H.; Aksay, I. A.; Liu, J.; Lin, Y. H. Glucose Oxidase-Graphene-Chitosan Modified Electrode for Direct Electrochemistry and Glucose Sensing. *Biosens. Bioelectron.* **2009**, *25*, 901−905.
(40) Zhang, R. X.; Fan, L. Z.; Fang, Y. P.; Yang, S. H. Electrochemical Route to the Preparation of Highly Dispersed Composites of ZnO/Carbon Nanotubes with Significantly Enhanced Electrochemiluminescence from ZnO. *J. Mater. Chem.* **2008**, *18*, 4964−4970.
(41) Huang, H. P.; Li, J. J.; Zhu, J. J. Electrochemiluminescence Based on Quantum Dots and Their Analytical Application. *Anal. Methods* **2011**, *3*, 33−42.
(42) Wang, L.; Xu, S. L.; Li, H. B.; Yue, Q. L.; Gu, X. H.; Zhang, S. Q.; Liu, J. F. Study for the Electrochemical Deposition on Single Carbon Fiber and Electrochemiluminescence of ZnO Nanostructures. *CrystEngComm* **2013**, *15*, 8444−8449.
(43) Keith, L.; Telliard, W. Priority Pollutants: I-a Perspective View. *Environ. Sci. Technol.* **1979**, *13*, 416−423.
(44) Shiu, W. Y.; Ma, K. C.; Varhanickova, D.; Mackay, D. Chlorophenols and Alkylphenols: A Review and Correlation of Environmentally Relevant Properties and Fate in an Evaluative Environment. *Chemosphere* **1994**, *29*, 1155−1224.
(45) Cheng, C. M.; Huang, Y.; Tian, X. Q.; Zheng, B. Z.; Li, L.; Yuan, H. Y.; Xiao, D.; Xie, S. P.; Choi, M. M. F. Electrogenerated Chemiluminescence Behavior of Graphite-like Carbon Nitride and Its Application in Selective Sensing Cu^{2+}. *Anal. Chem.* **2012**, *84*, 4754−4759.
(46) Dai, H.; Chi, Y. W.; Wu, X. P.; Wang, Y. M.; Wei, M. D.; Chen, G. N. Biocompatible Electrochemiluminescent Biosensor for Choline Based on Enzyme/Titanate Nanotubes/Chitosan Composite Modified Electrode. *Biosens. Bioelectron.* **2010**, *25*, 1414−1419.
(47) Yan, Y. T.; Liu, Q.; Wang, K.; Jiang, L.; Yang, X. W.; Qian, J.; Dong, X. Y.; Qiu, B. J. Enhanced Peroxydisulfate Electrochemiluminescence for Dopamine Biosensing Based on Au Nanoparticle Decorated Reduced Graphene Oxide. *Analyst* **2013**, *138*, 7101−7106.
(48) Yang, S. L.; Liang, J. S.; Luo, S. L.; Liu, C. B.; Tang, Y. H. Supersensitive Detection of Chlorinated Phenols by Multiple Amplification Electrochemiluminescence Sensing Based on Carbon Quantum Dots/Graphene. *Anal. Chem.* **2013**, *85*, 7720−7725.
(49) Liu, Q.; Wang, K.; Huan, J.; Zhu, G. B.; Qian, J.; Mao, H. P.; Cai, J. R. Graphene Quantum Dots Enhanced Electrochemiluminescence of Cadmium Sulfide Nanocrystals for Ultrasensitive Determination of Pentachlorophenol. *Analyst* **2014**, *139*, 2912−2918.

DOI: 10.1021/am507163z
ACS Appl. Mater. Interfaces 2015, 7, 3093−3100